

# *TWIST*: Research Proposal

## Executive Summary

- The *TWIST* collaboration has reached an intermediate goal by publishing results for three muon decay parameters ( $\rho$ ,  $\delta$ , and  $\mathcal{P}_\mu\xi$ ) with precisions a factor of two to three better than any prior experiments.
- The major systematic uncertainties have been addressed, and the experiment is in the final stages of data taking, which should be complete in 2007. The realization of the original goals of *TWIST*, to improve all three parameters by at least one order of magnitude compared with previous experiments, is within our reach.
- We have excellent students who will analyze the data, and with continued funding, the resources are in place to complete the experiment successfully.

## 1 Introduction

*TWIST*, the TRIUMF Weak Interaction Symmetry Test, is in the process of measuring the parameters describing the energy and angle distributions (with respect to muon spin) of positrons ( $e^+$ ) from positive muon ( $\mu^+$ ) decay. These muon decay parameters, or Michel parameters (after Prof. L. Michel [1]), offer a compact and convenient description of the electroweak interaction in muon decay.

This proposal describes the methods by which we measure the Michel parameters and why they are significant. We have already increased the experimental precision for the  $\rho$  [2],  $\delta$  [3], and  $\mathcal{P}_\mu\xi$  [4] parameters by factors of 2.5, 2.9, and 2.2 respectively, and are now in the process of further improving these results. New measurements of  $\rho$  and  $\delta$  are expected within six months, based on data taken in 2004. The eventual goal of *TWIST* is to improve all three parameters by at least one order of magnitude compared with previous experiments; that appears to be possible with the data which are being collected now. We explain what we have learned about the challenges to be faced in the minimization of the different sources of systematic errors, summarizing recent progress toward our objectives and outlining what remains to be done. *TWIST* will complete the data acquisition phase in 2007, and will concentrate on an analysis which reliably estimates and minimizes systematic uncertainties.

## 2 Physics Motivation

The Standard Model of the strong, weak and electromagnetic interactions, based on the gauge group  $SU(3)_C \times SU(2)_L \times U(1)_Y$ , has proven to be remarkably successful in describing the existing experimental observations. At present, there exist no experimental results that deviate from its expectations, with the exception of neutrino oscillations which could be considered to result from an extension to the mass matrices. However, the Standard Model is universally believed to be an incomplete theory of nature in spite of its many successes, and many extensions have been proposed.

Normal muon decay  $\mu \rightarrow e\nu\bar{\nu}$  is a process which is exceptionally well suited to studies of the space-time structure of the weak interaction. This comes about because the purely leptonic nature of the decay eliminates many uncertainties due to the internal structure of the particles or to contributions from other interactions.

By assuming a completely general, local, derivative-free, lepton-number-conserving, four-fermion point interaction, the matrix element for muon decay can be written in the charge-changing form as [5, 6]:

$$M = \frac{4G_F}{\sqrt{2}} \sum_{\substack{\gamma=S,V,T \\ \varepsilon,\mu=R,L}} g_{\varepsilon\mu}^\gamma \langle \bar{e}_\varepsilon | \Gamma^\gamma | (\nu_e)_n \rangle \langle (\bar{\nu}_\mu)_m | \Gamma_\gamma | \mu_\mu \rangle \quad (1)$$

This includes scalar, vector, and tensor ( $\Gamma^S, \Gamma^V, \Gamma^T$ ) interactions among charged lepton spinors of definite chirality ( $\varepsilon, \mu = R$  or  $L$ ). There are 10 complex amplitudes  $g_{\varepsilon\mu}^\gamma$  ( $g_{LL}^T$  and  $g_{RR}^T$  are zero), resulting in 19 independent real parameters. In the Standard Model,  $g_{LL}^V = 1$  and all others are zero (a  $V - A$  interaction). Constraints on the values of the coupling constants are derived from observables, such as muon decay positron spectrum and positron spin correlations, and the cross section for inverse muon decay.

Under the same assumptions, neglecting neutrino masses and radiative corrections, averaging over the polarization of the decay  $e^+$ , the differential decay rate of the positive muon is expressed as [1, 7, 8]

$$\frac{d^2\Gamma}{dx d\cos\theta} = \frac{1}{4} m_\mu W_{\mu e}^4 G_F^2 \sqrt{x^2 - x_0^2} \{ \mathcal{F}_{IS}(x) + \mathcal{P}_\mu \cos\theta \cdot \mathcal{F}_{AS}(x) \} \quad (2)$$

where

$$W_{\mu e} = \frac{m_\mu^2 + m_e^2}{2m_\mu} \quad x = \frac{E_e}{W_{\mu e}} \quad \mathcal{P}_\mu = |\vec{\mathcal{P}}_\mu|$$

$$x_0 = \frac{m_e}{W_{\mu e}} \quad \cos\theta = \frac{\vec{\mathcal{P}}_\mu \cdot \vec{p}_e}{|\vec{\mathcal{P}}_\mu| |\vec{p}_e|}$$

The isotropic and asymmetric parts, respectively, in the decay rate are written in terms of the decay (Michel) parameters  $\rho$ ,  $\eta$ ,  $\delta$ , and  $\xi$ .

$$\mathcal{F}_{IS}(x) = x(1-x) + \frac{2}{9}\rho(4x^2 - 3x - x_0^2) + \eta x_0(1-x) \quad (3)$$

$$\mathcal{F}_{AS}(x) = \frac{1}{3}\xi\sqrt{x^2 - x_0^2} \left[ 1 - x + \frac{2}{3}\delta \left\{ 4x - 3 + \left( \sqrt{1 - x_0^2} - 1 \right) \right\} \right] \quad (4)$$

$$(5)$$

Radiative corrections to the distribution are substantial, and must be incorporated. Corrections have been calculated including full  $O(\alpha)$  radiative corrections with exact electron mass dependence, leading and next-to-leading logarithmic terms of  $O(\alpha^2)$ , leading logarithmic terms of  $O(\alpha^3)$ , corrections for soft pairs, virtual pairs, and an ad-hoc exponentiation [9, 10, 11]. The result is adequate for measurements with a precision better than  $10^{-3}$ , and higher order estimates, motivated by the sensitivity of *TWIST*, can be performed.

The Standard Model predicts the decay parameters to take the values  $\rho = \frac{3}{4}$ ,  $\eta = 0$ ,  $\delta = \frac{3}{4}$ , and  $\xi = 1$ . The actual values of the parameters are very sensitive to the Standard Model assumption that the interaction is pure left-handed vector ( $V - A$ ); if terms with other characteristics

are present, the parameters differ. These decay parameters, and combinations of them, can be written in terms of bilinear combinations of the more general and fundamental coupling constants  $g_{\varepsilon\mu}^\gamma$ , such that deviations from Standard Model values will place very model independent limits on the individual couplings. The first measurements of the *TWIST* collaboration [2, 3] have already been included in a global analysis of muon decay data to tighten the constraints [6, 12].

Fetscher *et al.* [5] expressed the relationship in terms of probabilities  $Q_{\varepsilon\mu}$  ( $\varepsilon, \mu = R, L$ ) for a  $\mu$  handed muon to decay into a  $\varepsilon$  handed electron:

$$Q_{\varepsilon\mu} = \frac{1}{4}|g_{\varepsilon\mu}^S|^2 + |g_{\varepsilon\mu}^V|^2 + 3(1 - \delta_{\varepsilon\mu})|g_{\varepsilon\mu}^T|^2$$

To demonstrate how the Michel parameters can be used in a model independent test for handedness of the muon coupling, the probability for a right-handed muon coupling can be written as:

$$\begin{aligned} Q_R^\mu &\equiv Q_{RR} + Q_{LR} \\ &= \frac{1}{4}|g_{LR}^S|^2 + \frac{1}{4}|g_{RR}^S|^2 + |g_{LR}^V|^2 + |g_{RR}^V|^2 + 3|g_{LR}^T|^2 \\ &= \frac{1}{2}\left[1 + \frac{1}{3}\xi - \frac{16}{9}\xi\delta\right] \end{aligned} \quad (6)$$

The best measurements prior to *TWIST* were [6]:

$$\begin{aligned} \rho &= 0.7518 \pm 0.0026 & \mathcal{P}_\mu \xi &= 1.0027 \pm 0.0079 \pm 0.0030 \\ \eta &= -0.007 \pm 0.013 & \mathcal{P}_\mu \frac{\xi\delta}{\rho} &> 0.99682 \\ \delta &= 0.7486 \pm 0.0026 \pm 0.0028 \end{aligned}$$

The first two publications from *TWIST* [2, 3] reduce the uncertainties in  $\rho$  and  $\delta$  by factors of 2.5 and 2.9 respectively. The Review of Particle Physics [6] now identifies them as the best available. More recently, we have published a direct measurement of  $\mathcal{P}_\mu \xi$  which is a factor of 2.2 more precise [4].

The main goal of *TWIST* is to search for new physics through more precise measurements of the muon decay parameters. We aim to set new limits on the right-handed coupling of the muon in a model independent way, as well as to squeeze the parameter space for classes of extensions to the Standard Model, such as those invoking left-right symmetry, with less model dependence than otherwise possible.

Left-right symmetric (LRS) models include a heavier partner to the standard  $W_1$  boson, a  $W_2$  which has mostly right handed coupling. Mixing of the two bosons of mass  $m_1$  and  $m_2$ , with angle  $\zeta$ , leads to small deviations of  $\rho$  and  $\xi$  from the Standard Model values:

$$\frac{3}{4} - \rho \approx \frac{3}{2} \left( \frac{g_R}{g_L} \zeta \right)^2 \quad (7)$$

$$\frac{1 - \mathcal{P}_\mu \xi}{4} \approx 2 \left[ \left( \frac{g_R m_1}{g_L m_2} \right)^4 + \left( \frac{g_R}{g_L} \zeta \right)^2 \right] \quad (8)$$

where  $g_R$  and  $g_L$  are the right- and left-handed gauge couplings. Other experiment are sensitive to LRS interactions. Some examples are direct searches for a right-coupling  $W$  at high energies, the  $K_L - K_S$  mass difference, CKM unitarity, and  $\beta$  decay. All involve hadrons, while muon

decay is purely leptonic (except that the muon's polarization comes from pion decay). For this reason, muon decay limits need not make assumptions about the right-handed CKM matrix ( $g_R$ ), but can include the dependence explicitly. Our current LRS limits are shown in Section 4.

The relationship of muon decay parameters to neutrino mass limits has been investigated by the Caltech group [13]. With certain assumptions, some of the LR coupling constants in the model-independent analysis of [5] are strongly constrained. The same group has studied supersymmetric decay contributions to weak decay correlations [14]. While the three parameters which *TWIST* can access are likely not sensitive to these particular supersymmetric models, the fourth parameter,  $\eta$ , appears to be more interesting.

In this experiment  $\mathcal{P}_\mu$  is the magnitude of the  $\mu^+$  polarization along the beam axis at the time of muon decay. Surface  $\mu^+$  [15], which are muons produced from  $\pi^+$  decays at rest, have a polarization of magnitude  $\mathcal{P}_\mu^\pi$ , in a direction antiparallel to their momentum. In the SM with massless neutrinos  $\mathcal{P}_\mu^\pi = 1$ . In this experiment  $\mathcal{P}_\mu\xi$  is determined from the positron spectrum, while  $\mathcal{P}_\mu^\pi\xi$  must take into account any depolarization using, for example, the measurements of the muon trajectories.

### 3 The *TWIST* Spectrometer

The *TWIST* detector is described in detail in [16], and the beam monitoring time expansion chamber (TEC) system is described in [17]. The latter is included as a supporting document. This section provides only a summary of those articles, with the inclusion of extra information on the spectrometer solenoid and on the muon source.

The spectrometer detector consists of a symmetric array of planar detectors, called the detector stack, which is constructed to very high precision with attention paid to minimizing the amount of material in the tracking region. At the center of the array is a thin target in which the muons stop. This allows very precise measurement of positron decay tracks while minimizing interactions which would broaden and distort the detector response function. The planar geometry means that the energy loss, which depends on the length of a track in any material in its path, has a simple  $1/|\cos\theta|$  dependency.

The detector stack is in a very uniform solenoidal field of 2 T. A thin scintillator records the incoming muon, providing an unbiased trigger for events. The incident beam characteristics and the beam entrance path are engineered so as to minimize depolarization, the knowledge of which is crucial in setting limits on  $\mathcal{P}_\mu\xi$ , as it will affect the difference between  $\mathcal{P}_\mu^\pi$  and  $\mathcal{P}_\mu$ . The material of the stopping target is also chosen to minimize known sources of depolarization due to interactions of the muon with its environment prior to decay.

A conceptual cutaway view of the spectrometer is shown in Fig. 1.

#### 3.1 The detector array

The detector stack consists of 56 low-mass high-precision planar wire chambers. The original placement of the chamber planes is shown in Fig. 2. The spacing between planes has since been adjusted to make the spacings less uniform, to help resolve an annoying ambiguity in helix pitch determination. This change has significantly reduced the effect of tracking errors at a particular value of longitudinal momentum that was within our fiducial.

*TWIST* uses two types of wire chamber detectors, which we call DCs with 4 mm wire spacing and PCs with 2 mm spacing. Both types measure either the  $u$  or  $v$  coordinate, in a system rotated by  $\pi/4$  from the horizontal-vertical ( $x, y$ ) system.

The DC planes are arranged in modules, the simplest of which is a UV module consisting of a pair of DC planes. There are 14 of these in sparsely spaced arrays, 7 on each side of the target module. The remainder of the 44 DC planes are assembled into two densely stacked modules, at either end of the sparse arrays of UV modules. DCs use a slow gas (dimethyl ether, or DME) to achieve excellent position resolution. Their function is to determine precisely the coordinates of

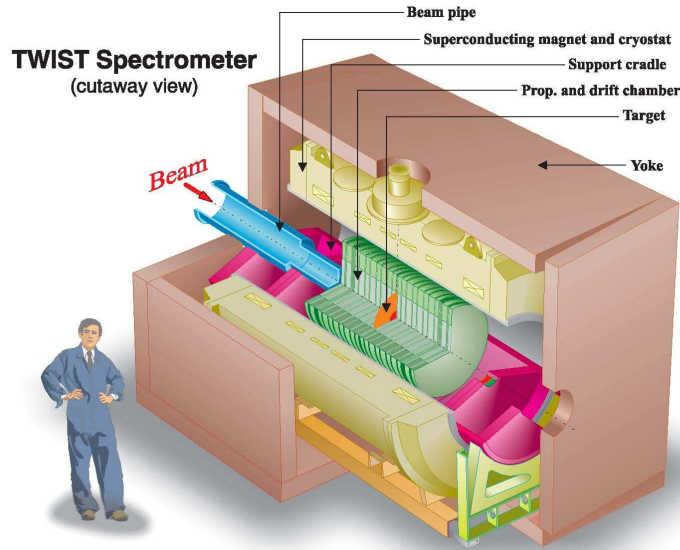


Figure 1: Conceptual drawing of the *TWIST* spectrometer. It shows the superconducting solenoid within the steel yoke, with the drift chambers and proportional chambers symmetrically placed about the central target.

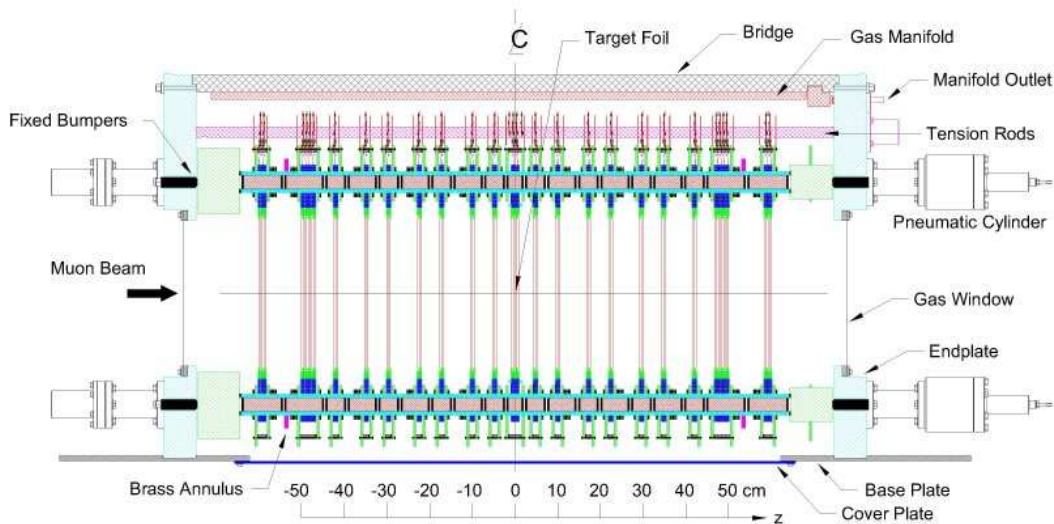


Figure 2: Side view of the symmetric *TWIST* detector stack, showing 19 modules at precise locations along the beam axis.

the decay positron path. The sparse arrays of UV planes near the muon stopping target (DC9-DC22 US, and DC23-DC36 DS) are spaced to minimize scattering between planes while giving some redundancy of measurement. The dense stacks of DCs (DC1-DC8 US and DC37-DC44 DS) help to resolve any pitch ambiguities in tracks.

PC chambers are arranged in three modules. They serve to identify the primary character-

istics of an event and to identify the times of each track in a window  $[-6, +10] \mu\text{s}$  with respect to the time of a simple thin scintillator event trigger. Four PC planes in each of two modules, one at the upstream (US, PC1-PC4) and another at the downstream (DS, PC9-PC12) ends of the stack identify decay positrons; if both groups are hit, a penetrating beam positron is the likely source. Pulse widths can also be used to separate positrons from more highly ionizing tracks. Four additional PC planes (PC5-PC8) are part of the target module and surround the muon stopping target (changed in September 2006 from  $71 \mu\text{m}$  high purity 5N Al to  $29 \mu\text{m}$  high purity 5N Ag, as a confirmation of the target depolarization systematic), which acts also as a cathode for PC6 and PC7. Muons stopping in the target satisfy  $\text{PC6} \cdot \overline{\text{PC7}}$ .

Planes are positioned with extreme accuracy of  $5 \times 10^{-5}$  in the  $z$  (beam and magnetic field) direction, using specially constructed glass ceramic spacers. Alignment in the transverse  $u, v$  directions is accomplished with fits of straight tracks, but depends also on the relative wire separation accuracy which was measured with rms value of  $\sigma = 3.3 \mu\text{m}$  for 6,304 sense wires in the chamber modules (including spare modules).

Apart from the muon stopping target, the materials of the stack in the particle path are only the anode wires,  $6.2 \mu\text{m}$  aluminized Mylar cathode foils defining the chamber planes, chamber gas, and He gas with a small nitrogen content in the spaces between modules. Each detector plane has a thickness of only about  $5 \times 10^{-5}$  radiation lengths. For a more complete description of construction details, see [16].

The nominal field of 2 T is produced by a superconducting solenoid which was originally constructed about twenty years ago as an early-generation whole body MRI field device, with an added external steel yoke. Within the tracking DC volume ( $|z| < 500 \text{ mm}$ ,  $r < 160 \text{ mm}$ ), field map measurements at 2.0 T determine the variations of the field as a function of position to  $5 \times 10^{-5}$ . The field is uniform over the full volume to  $4 \times 10^{-3}$  (full width). It has also been mapped at 1.96 T and 2.04 T. Separate overlapping field maps were made for the tracking region and the muon entrance region where fringe field depolarization is important. An OPERA-3D field simulation, tuned and verified to the measurements, is used to create the full field maps used for tracking and event simulation production.

### 3.2 The time expansion chamber system

The need for efficient and accurate characterization of the muon beam has led to the development and construction of a low-pressure, low-mass transverse drift chamber dubbed the time expansion chamber, or TEC [17]. A depiction of the device is shown in Fig. 3. It consists of two modules, one to measure in each of the  $x$  and  $y$  directions, which are enclosed in a chamber with 0.080 bar of DME. Thin ( $6.25 \mu\text{m}$ ) aluminized Mylar windows isolate the chamber from the beam line vacuum along the axis of the chamber. It is coupled directly into the beam line approximately half way between the last quadrupole element and the entrance to the solenoid yoke. Each of the  $x$  and  $y$  modules consists of a region of uniform transverse electric field in which the ionization drifts to 24 sense wires in multiplication regions to one side of the particle track. The time of arrival of ionization at the sense wires with respect to external detection of the beam particle (*e.g.*, by the muon trigger scintillator) determines the distance from the sense wire. Thus the position and angle of each track is measured by fitting up to 24 individual position measurements in each module.

The TEC is located near the entrance to the solenoid, in a region where the fringe field is about 0.1 T, mostly in the direction of the beam particles. Even though it has very low mass, the scattering from windows, gas, and field cage wires will reduce the muon polarization by scattering, so it is not in place while the majority of spectrometer data are being collected. However, it is made so that it can be reproducibly installed or removed in a few hours, to perform regular checks of beam position and divergence distributions. This serves to monitor systematic variations in the muon beam which will affect the precision of decay parameter measurements. We typically insert the TEC to characterize the beam near the beginning and the end of each data set, or if a change in the muon beam is anticipated due to circumstances beyond our control

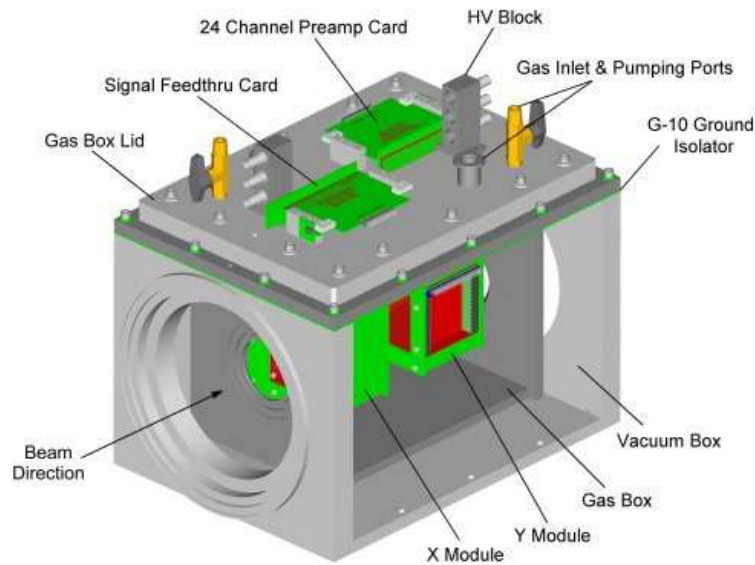


Figure 3: The TEC, showing two modules which measure the position and angle of beam particles, one in  $x$  and one in  $y$ .

(muon production target change, proton beam tune change). Between beam characterization runs with the TEC, while muon decay data are being taken, we rely on careful monitoring of many quantities, including the muon beam envelopes as measured by the DCs in the upstream half of the detector stack. For a few data sets, we leave the TEC in place to confirm our ability to identify beam changes based on other non-TEC information.

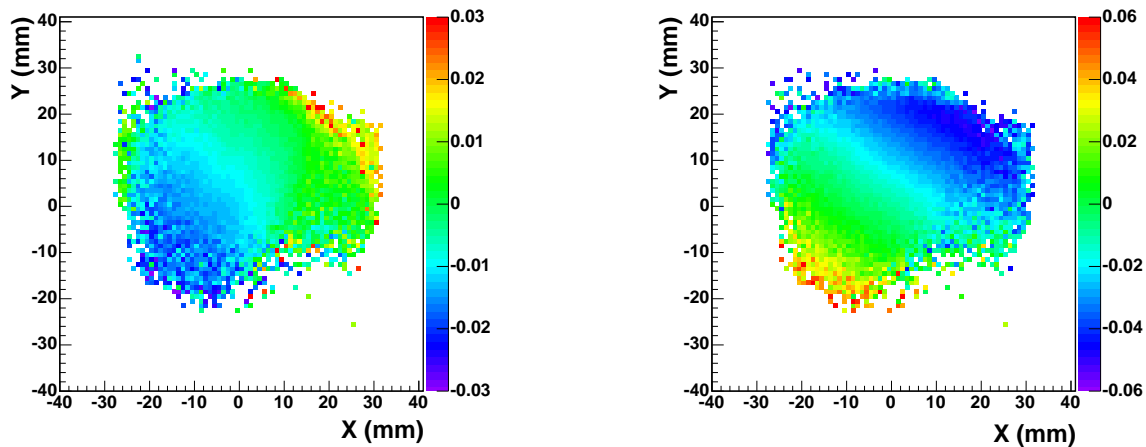


Figure 4: Two-dimensional distributions of the muon beam mean angle with respect to the  $z$  axis in the  $xz$  plane ( $\theta_x$ , left) and in the  $yz$  plane ( $\theta_y$ , right). The color scales, representing the angles in radians, are different to show the trends more clearly. The plots show the rotation of the angle-position correlation due to the fringe field of the solenoid, and the smaller divergence of the beam in the  $x$  direction than in  $y$  for this particular beam tune.

An example of a beam measurement, for surface muons from a graphite primary pion production target, is shown in Fig. 4. The correlations of angles with beam position allow a precise simulation of the muon beam entering the solenoid. The simulation uses as input a beam in

which the effects of multiple scattering prior to and during passage through the TEC are removed by a quadratic subtraction technique, performed for each of many subregions in the  $xy$  two-dimensional distribution. For more details, see [17].

### 3.3 The muon source

Muons for *TWIST* are produced from positive pions ( $\pi^+$ ) decaying at rest, at or near the surface of the pion production target (surface muons [15]). For a massless left-handed neutrino, the absence of non-Standard Model interactions leads to a positive muon ( $\mu^+$ ) with spin antiparallel to the momentum direction. The result is that surface muons have a high polarization in a direction opposite to the beam direction. Several factors contribute to a difference of the polarization from the ideal value. Most are controlled via a high quality, low emittance beam transport system, the M13 beam line, from the pion production target to the *TWIST* solenoid entrance.

Scattering of muons changes the momentum direction but not the spin direction, which would lead to depolarization of the beam. If this happens in the high solenoidal field of the *TWIST* spectrometer, the momentum direction has already become irrelevant to the spin distribution as measured, but if it happens before entering the solenoid, it is important. By choosing muon momenta near the kinematic limit of 29.79 MeV/c, the small momentum acceptance of  $\sim 1\%$  allows only very small depolarization from scattering within the pion (and muon) production target. Finite acceptance of the channel leads to a distribution of spin directions about the mean beam direction. A small and well-characterized emittance make this depolarization small and easily estimated.

Depolarization may also occur in the interactions of muons during and/or after thermalization in the muon stopping target or nearby materials. Demanding that we accept only muons which stop in the production target or the last preceding detector plane, PC6 (*i.e.*, requiring PC6 · PC7) purifies the data sample; those which stop in PC6 can be largely removed by cuts on ionization in PC5 and PC6, as will be discussed in a Section 4.7.4. Depolarization of muons when slowing from  $p = 29.6$  MeV/c down to zero is discussed in [18, 19, 20, 21]. For muons which do stop in the target (Al or Ag), the effect is negligible if the incident muon has a kinetic energy of at least  $\sim 100$  keV when it enters. Simulations show this to be true for over 99% of the muons stopping in the Al target.

A significant potential source of depolarization for *TWIST* is the effect of the fringe field as the muon enters the solenoid. The radial field components impart transverse momentum (and spin components) to any trajectory which does not follow a field line. This can be minimized by choosing the size and divergence of the beam appropriately, and by minimizing the mean muon transverse momentum in the solenoid. The remaining apparent depolarization can be reliably predicted by knowing both the beam characteristics (size, divergence, momentum, and correlations between them) and the fringe field spatial dependence.

The M13 muon beam line has been improved in several ways to improve *TWIST* data. The most recent upgrade was the installation of asymmetric current supplies to three of the M13 quadrupoles to allow more control of the muon beam. Used in conjunction with the final B2 bending magnet, they allow the beam to be steered to optimal mean positions and angles ( $x$ ,  $y$ ,  $\theta_x$ ,  $\theta_y$ ), ideally near zero so as to coincide with the solenoid field symmetry axis. In Fig. 4, the mean values especially for  $y$  and  $\theta_y$  are not sufficiently close to zero for our needs, due to an unforeseen effect of the solenoid fringe field on the muon beam in M13. With quadrupole steering, it is possible to reduce the mean values substantially and to tune the beam parameters to achieve a minimum in the mean transverse muon beam momentum in the upstream DCs (see Section 5.1.2).

From the outset, a gas degrader of length 20 cm has been in the muon path inside the solenoid, following a vacuum isolation window and immediately before the beam passes through the trigger scintillator and enters the detector stack. Since all of the materials are in the high field region, muon scattering does not cause appreciable depolarization. A variable mixture of

He and CO<sub>2</sub> is adjusted so that the muon stopping position as measured by the detector planes is in the correct place. Because atmospheric density variations cause the position to move slightly, the gas composition is automatically adjusted based on measurements of mean muon stopping position, to compensate for their variations and to keep the muon stopping position precisely located.

## 4 Data Analysis and Results

### 4.1 Analysis methodology

The challenge in the analysis is to select the  $e^+$  emitted from  $\mu^+$  decays over the largest possible range of momentum and angle without introducing significant bias. This analysis is applied both to the data and the simulation, and the results are compared to determine the decay spectrum. Biases in the analysis are then compensated to the extent with which the simulation accurately reproduces the data. The validation of the simulation then determines the associated systematic uncertainty.

Cuts based on the decay time do not produce angle/momentum biases. Uncertainties in the determination of the decay time for different tracks are essentially determined from our calibration of the time offsets for the chamber wires, and are rather small. However cuts based on geometry clearly can produce such biases. The need for geometry based track selection is primarily driven by the presence of multiple tracks such as deltas or hard scatters. The identification and reconstruction of all tracks in this kind of event reduces sensitivity to the comparative rates of such events in the data and the simulation.

The *TWIST* detector has an intrinsic granularity determined by the plane and wire spacings, which was significantly reduced by the rearrangement of detector planes mentioned previously. A consequence of this granularity can be understood by considering the track of a helix with pitch equal to twice the average plane pair spacing. The  $z$ -projection of such a track is a circle with the hits clustered at diametrically opposite points, so the circle radius is poorly determined. Such tracks challenge the pattern recognition and require the full accuracy of the helix fitter. This results in some momentum-angle tracks being less well defined. The fiducial region is then chosen to eliminate these tracks. Considerations such as these drive the analysis strategy to minimize the sensitivity of our analysis to decays that are more difficult to simulate.

Key elements of our analysis are:

- *Crosstalk removal*: This uses primarily the time width of the hit signals, but also checks for the existence of a generating signal. Only for the large ionization produced by muons is this effect significant.
- *Windowing*: Hits are separated into temporally isolated groupings using PC and DC information.
- *Classification*: Possible kinds of tracks within each window are identified by the topology of the hits. For the vast majority of events this topology is primarily temporal.
- *Pattern Recognition*: Tracks are identified through a fit to a helix of space points determined from clusters of wire hits within a window. More than one track candidate can be reported for each window. Delta ray tracks, which follow the magnetic field direction, are also identified.
- *Wire center fits*: Helices are fit to the wire positions using the “narrow windows” technique [22]. Multiple scattering is included by allowing kinks at each sparse UV chamber pair position, constrained by the multiple scattering distributions [23]. The resulting fit has sufficient precision to resolve most left-right ambiguities.

- *Track fitting:* The particle trajectories are determined from fits to the hit times in the drift chambers incorporating space-time relations (STRs) calculated from GARFIELD. The variable step size arc approximation is employed to integrate over the measured magnetic field map, and kinks are again introduced to account for multiple scattering.
- *Tree output:* Unbinned results of this analysis including track momenta and angle, classification and window information are output to ROOT trees (equivalent to hbook ntuples).
- *Energy calibration:* A fit to the upper edge of decay positron histograms in angle and energy derived from these trees is performed to correct the positron momenta for energy losses in the spectrometer, which have a  $1/|\cos\theta|$  dependence on the decay angle. This fit also tests for a possible error in overall momentum scale.
- *Michel fits:* 2D histograms, binned using the energy calibration, are produced with appropriate fiducial cuts. These histograms are fit to analogous histograms from the simulation generated using hidden Michel parameters and their derivative distributions.

## 4.2 Calibrations

Calibration procedures have been refined during the past year. Our ability to calibrate is closely correlated to our ability to track. Calibration of the the relative TDC times can now be done both with straight and helical tracks. The fitting of 120 MeV/c pion tracks in zero magnetic field is used to determine translational and rotational alignments of chamber planes. Distortion in helical tracks from the expected shape is used to determine the orientation of the chambers to the magnetic field map.

See Section 5.3 for a discussion of energy calibrations.

## 4.3 Simulation code

The current simulation code has been developed using GEANT 3.21. This simulation has an accurate description of the materials in and near the tracking region of the detector. The simulation incorporates a realistic distribution of charge clusters produced by ionization in the chambers, leading to reasonable simulation of the observed spatial resolution. Detector translational and rotational (mis)alignments have been included in the simulation. The muon beam is simulated according to the emittances measured in the TEC for the specific run conditions. The TEC is fully implemented within the simulation, allowing for an accurate determination of these emittances, and thus of the effective muon polarization.

## 4.4 Extraction of decay parameters and blind analysis

To extract decay parameters from the experimental momentum and angle decay positron spectrum, one needs to take into account detector response. In *TWIST*, the convolution of the reconstructed spectrum is calculated directly by a simulation program without the explicit knowledge of detector response. However a simulation requires not just the theoretical formula, but also a set of specific values of decay parameters to proceed, and the result is a convolution just for those values. To perform a fit for non-specific values of decay parameters, *TWIST* has developed a technique which uses an expansion of the convoluted spectrum in deviations of the parameters from their MC values. The scheme can be visualized by

$$n_i(\alpha_{\text{Data}}) = n_i(\alpha_{\text{MC}}) + \frac{\partial n_i}{\partial \alpha} (\alpha_{\text{Data}} - \alpha_{\text{MC}}),$$

where  $n_i(\alpha_{\text{Data}})$  is the experimental spectrum,  $n_i(\alpha_{\text{MC}})$  is the simulated one, and  $\Delta\alpha = \alpha_{\text{Data}} - \alpha_{\text{MC}}$  is the fit parameter. The  $\partial n_i / \partial \alpha$  coefficient is calculated by Monte Carlo using analytical

derivatives of the theoretical spectrum, where  $\alpha$  stands for the decay parameters  $\{\rho, \eta, \xi, \xi\delta\}$ . Since the Michel form of the spectrum is linear in  $\alpha$ , the first-order expansion is exact in this parametrization. The simulated spectrum in the above description is in fact made up from *reconstructed* Monte Carlo events.

The fitting procedure described above allows for a straightforward “blinding” of the analysis: since the fit gives only the deviations from the MC values, it is enough to hide  $\alpha_{MC}$ . The *TWIST* implementation of blind analysis uses asymmetric cryptography, and the only “secret” is the private key. Values of decay parameters for MC production are generated randomly, within given tolerances, and are used to produce a set of “decays”  $\{E, \cos(\theta)\}$  which is stored on disk and can be fed to GEANT.

The system is also applied to the estimation of biases and systematic effects, where differences in decay parameters are determined from comparisons of data sets (real data or simulation) obtained under differing controlled conditions. This procedure has been used for the current publications.

## 4.5 Computation logistics

Much of the development and testing of our analysis software has been accomplished using our local cluster of some 30 computers, about half of which are desktop workstations. Production analyses and simulations are performed using the WestGrid Glacier cluster of 1680 P4 processors. Our allocation on this resource has been sufficient to allow analysis of our data in a timely manner. We have developed scripts which greatly facilitate job submission and monitoring together with the associated documentation. We make considerable use of the storage resources at Glacier and SFU to archive our raw data and simulations. The local cluster machines are still used extensively for processing of ROOT trees, code development and testing, calibrations, and specialized analyses.

## 4.6 $\mathcal{P}_\mu^\pi \xi$ result from 2004 data

The result for  $\mathcal{P}_\mu^\pi \xi$  uses a data sample consisting of  $2 \times 10^9$  events recorded in Fall 2004. This data sample includes eight data sets, of which seven were used for the extraction of  $\mathcal{P}_\mu^\pi \xi$ . Simulations to fit each of the seven data sets used different beam characterization profiles, derived from beam measurements performed after the data collection, which matched different conditions under which the data were recorded. The remaining data set was used to determine the detector response using decay positrons from muons stopping in the trigger scintillator and the first few chamber planes (far upstream), as described in [2, 3]. A complete description of the  $\mathcal{P}_\mu^\pi \xi$  measurement can be found in [4], submitted as a supporting document with this application; a summary is presented below.

Five sets of data were taken with the beam steered nominally. One data set had the muon beam stopping with the Bragg peak centered in the target (stop  $\frac{1}{2}$ ). Two sets, which were separated in time by a few days, were taken with the muon Bragg peak shifted to  $3/4$  of the way through the Al stopping target (stop  $\frac{3}{4}$  A, B). One set was taken with a muon beam size limiting aperture (aperture), and one set was taken with the beam rate increased (high rate). Two sets of data were collected with the beam displaced by changing the last bending magnet (B2) field by  $+0.5\%$  from nominal. One of the data sets (B2+0.5%) had the muon Bragg peak centered in the stopping target, while in the other set (PC5 stop), the muons were stopped relatively far upstream in order to increase the relative fraction of muons stopping in gas.

The systematic uncertainties in the measurement of  $\mathcal{P}_\mu^\pi \xi$  are presented in Table 1, taken from [4]. Several of the systematic uncertainties could vary from data set to data set and are denoted by (ave). They are considered data set dependent when calculating the weighted average value of  $\mathcal{P}_\mu^\pi \xi$ . For example, the effect of positron interactions on upstream and downstream

decay positrons changes when the mean muon stopping location is adjusted; thus the systematic uncertainty due to positron interactions is set-dependent. Two of the leading contributions in Table 1 arise from potential sources of muon depolarization, while a third is due to chamber response. They are described in the following paragraphs; more details of all contributions are in the publication.

Table 1: Contributions to the systematic uncertainty for  $\mathcal{P}_\mu^\pi\xi$ .

Effect	Uncertainty
Depolarization in fringe field (ave)	0.0034
Depolarization in stopping material (ave)	0.0012
Chamber response (ave)	0.0010
Spectrometer alignment	0.0003
Positron interactions(ave)	0.0003
Depolarization in production target	0.0002
Momentum calibration	0.0002
Upstream-downstream efficiency	0.0002
Background muon contamination (ave)	0.0002
Beam intensity (ave)	0.0002
Michel parameter $\eta$	0.0001
Theoretical radiative corrections	0.0001

The systematic uncertainty in the fringe field depolarization is estimated from the different settings used in data taking for the second dipole element (B2) in the M13 channel. The relative changes in angle and position between the nominal B2 value (94.6 mT) and B2+0.5% settings are similar for the two periods, but the absolute numbers for the average beam angles are quite different. This could be due to changes in the performance of the beam monitoring chamber or to its alignment to the beamline. To determine the sensitivity of the polarization to beam position and angle, a simulated beam was scanned in position and angle and using a parameterization of the results, the larger of the differences in predicted polarization for a given B2 setting (0.0033) is adopted as an estimate of the uncertainty due to limits of reproducibility. Uncertainties due to deconvolution of the beam angle measurement, modeling of the shape of the solenoid fringe field, and beam size reproduction also contribute to the final quoted systematic uncertainty of 0.0034 due to fringe field depolarization.

The depolarization of the muons while they propagate through the detector and interact with the detector materials is negligibly small for non-relativistic muons [20]. Muonium formation is suppressed by ensuring that the majority of the muons have sufficient energy entering the Al target. Most of the muons stop in the high-purity Al target, where they can interact with conduction electrons. These electrons create a hyperfine magnetic field at the site of the muon, which results in a Korringa depolarization rate [24, 25] that has an exponential form, and does not depend on the magnetic field. In this experiment 2.5% to 5.5% of the muons stop in the gas before the stopping target. The functional form of the depolarization in gases is unknown, thus an assumption that there is no unseen rapid depolarization is made. The spin relaxation, with mean lattice-site residence time  $\tau_c$ , is given approximately by the Kubo-Tomita expression [26], which reduces to Gaussian (exponential) forms for  $\tau_c \rightarrow \infty$  ( $\tau_c \rightarrow 0$ ). The difference between Gaussian and exponential extrapolations of the integral asymmetry measurement, as shown in Fig. 5, is  $2.4 \times 10^{-3}$ . Data before  $1.05 \mu\text{s}$  are not considered because of possible contamination of late TDC signals from muons for upstream decay positrons. Half the difference between the two different extrapolations is the *correction* applied to the simulation to data fits, because the simulation was generated with a Gaussian form, while in reality the shape is most likely a linear combination of a Gaussian and exponential. An estimate of the extrapolation uncertainty is half

the difference between the Gaussian and exponential extrapolations.

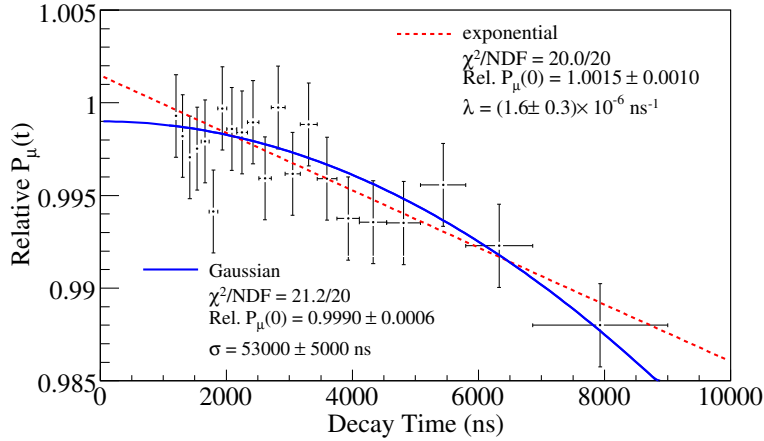


Figure 5: Extrapolation to zero decay time of relative muon polarization, estimated using the decay positron integral asymmetry described in the text. The extrapolation function is fit to data, with an exponential shown as a dashed line, and as a Gaussian shown as a solid line.

The chamber response systematic uncertainty in  $\mathcal{P}_\mu^\pi \xi$  comes from several sources, studied (as were many others) by employing fits of experimental data (or simulation) samples, taken with a systematic parameter set at an exaggerated level, to data (or simulation) taken under ideal conditions. The difference measured, or sensitivity, expresses the changes in the spectrum shape caused by the systematic effect in terms of the changes in the Michel parameters. For example, to estimate the possible variation in the wire to wire time offsets (time zero, or  $t_0$ ), calibration runs are taken at the beginning and end of the run period. To measure the sensitivity of the muon decay parameters to  $t_0$  variations, a calibration scaled by ten times the difference in the beginning and end of run time calibrations is used. The contribution due to  $t_0$  variations, obtained from fitting the exaggerated time shift analysis spectrum to a nominal spectrum, is  $0.89 \times 10^{-3}$ . Several other small effects are included in the chamber response systematic. Time variations in the shape of cathode foils due to variations in differential pressure (which we call the “foil bulge” systematic) is estimated to be  $0.22 \times 10^{-3}$ , based on our control of the bulge to better than  $50 \mu\text{m}$ . Construction variations among different DC planes, also causing variations in foil spacings, adds  $0.20 \times 10^{-3}$ , while environmental density changes lead to a systematic uncertainty of  $0.17 \times 10^{-3}$ . There is ionization from the passage of the incident muon in the upstream DCs, which may have some influence on positron track identification in the upstream DC array some microseconds later. This may lead to an uncertainty in  $\mathcal{P}_\mu^\pi \xi$  (which we call the “dead zone” systematic), conservatively estimated at  $0.01 \times 10^{-3}$  via a model of the effect based on DC measurements.

The spectrum fit results for the parameter  $\mathcal{P}_\mu^\pi \xi$  are presented in Table 2. At the present stage *TWIST* cannot provide an improved measurement of  $\eta$ , therefore its value is set to the global analysis value of  $-0.0036$  [12], to constrain the other parameters better. The uncertainty of  $\pm 0.0069$  on the accepted value of  $\eta$  gives an uncertainty of  $\pm 0.0001$  on the final value of  $\mathcal{P}_\mu^\pi \xi$ . To illustrate the quality of the fit, and how the spectrum fit distinguishes between  $\mathcal{P}_\mu^\pi \xi$  and  $P_\mu^\pi \xi \delta$ , the contribution to the fit asymmetry versus momentum for each of these terms and from the best fit  $A(p)$  are shown in Fig. 6. Note that the total asymmetry versus momentum,  $A(p)$ , is  $A(p) = A_\xi(p) + A_{\xi\delta}(p)$ , where  $A_\xi$  is the asymmetry when the  $P_\mu^\pi \xi \delta \cos \theta \frac{2}{3}(4x^3 - 3x^2)$  contribution to the positron decay spectrum is zero, and  $A_{\xi\delta}$  is the asymmetry when the  $P_\mu^\pi \xi \cos \theta (x^2 - x^3)$  contribution is zero. The top panel in Fig. 6 shows the best fit asymmetry versus positron momentum,  $A(p)$ , with all of the fiducial cuts applied as a solid line; the contribution to the fit

from the  $\xi$  term as a long-dashed line; and the contribution to the fit from the  $\xi\delta$  term as the short-dashed line. The bottom panel shows the difference,  $\Delta A(p)$ , between data and fit.

Table 2: Results for  $\mathcal{P}_\mu^\pi \xi$ . Each fit has 1887 degrees of freedom. Statistical and set-dependent systematic uncertainties are shown. A description of the data sets is in the text.

Data set	$P_\mu^\pi \xi \pm \text{stat} \pm \text{syst}$	$\chi^2$
B2+0.5%	$1.0023 \pm 0.0015 \pm 0.0037$	2007
PC5 stop	$1.0055 \pm 0.0030 \pm 0.0038$	1906
stop $\frac{1}{2}$	$1.0015 \pm 0.0014 \pm 0.0037$	1876
stop $\frac{3}{4}$ A	$0.9961 \pm 0.0014 \pm 0.0037$	1900
high rate	$0.9997 \pm 0.0019 \pm 0.0037$	1932
aperture	$0.9978 \pm 0.0018 \pm 0.0037$	1896
stop $\frac{3}{4}$ B	$1.0009 \pm 0.0019 \pm 0.0037$	1841

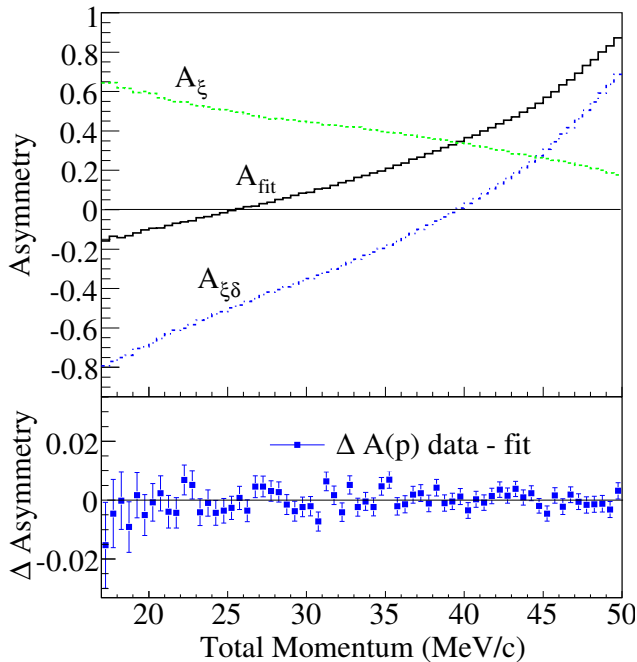


Figure 6: The top panel shows the fit asymmetry versus positron momentum,  $A(p)$ , along with the contributions to the fit  $A(p)$  from the  $\xi$  and  $\xi\delta$  terms. The bottom panel shows the difference between the data and fit,  $\Delta A(p)$ .

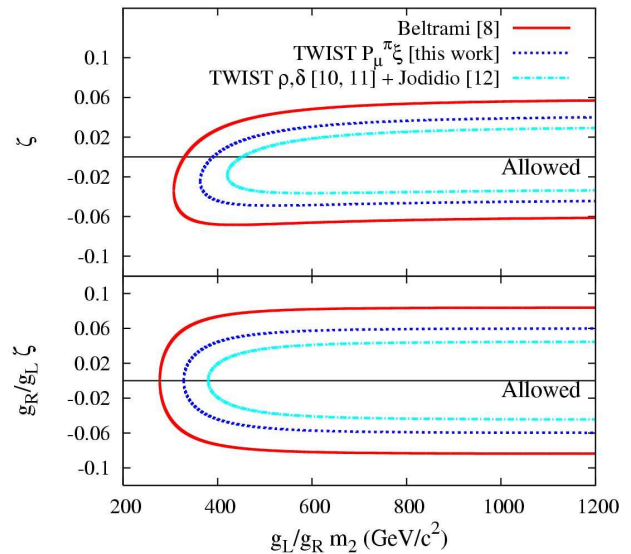


Figure 7: The top panel shows the manifest LRS model 90% confidence limits on  $\zeta$  and  $m_2$  ( $g_L/g_R = 1$ ) from measurements of  $\mathcal{P}_\mu^\pi \xi$ . The bottom panel shows the same limits in the general LRS model case.

The value of  $P_\mu^\pi \xi$  was determined to be  $1.0003 \pm 0.0006(\text{stat.}) \pm 0.0038(\text{syst.})$ . The central value for  $P_\mu^\pi \xi$  was calculated as a weighted average using a quadratic sum of the statistical and set-dependent uncertainties for the weights. The final systematic uncertainty is a quadratic sum of the set-independent and the average values of the set-dependent systematics.

The 90% confidence limits on the LRS model parameters from this measurement are  $-0.050 < \zeta < 0.041$  and  $m_2 > 360 \text{ GeV}/c^2$  in the manifest case, and  $-0.061 < g_R/g_L \zeta < 0.061$  and

$g_L/g_R m_2 > 325 \text{ GeV}/c^2$  in the general LRS model. The LRS model limits are shown in Fig. 7. The present result reduces the uncertainty on the direct measurement of  $\mathcal{P}_\mu^\pi \xi$  [27] by a factor of more than two; it is also consistent with the SM and the value obtained indirectly [2, 3, 18, 19].

## 4.7 Insights for systematics from 2005 data

The experiences gained from first analyses of the data from 2004 raised many issues. It was clearly necessary to dedicate beam time to tests specifically designed to resolve those issues, while at the same time planning and implementing improvements to the beam, the beam characterization, and our operating procedures. Some of the results are described in the following subsections.

### 4.7.1 Possible dependence of $\mathcal{P}_\mu \xi$ on solenoid B field

A difference of  $(15 \pm 2) \times 10^{-3}$  in polarization was observed between 2002 datasets where the solenoid field was changed from 1.96 T to 2.04 T. At that time we were using a graphite-coated Mylar muon stopping target. Subsequent simulations were done to study the effects of the change in the fringe field region and changes in the beam between these changed solenoid field data sets. The final polarization predicted by the simulation with these changed fringe fields and changed beams did not explain this large difference in polarizations as measured in the data. There is, however, a large uncertainty in the beam profiles used for the 2002 data such that we cannot completely rule out this scenario.

A more likely model for this large change in polarization between the 2002 data for the different solenoid field data sets is that different fractions of the muons were stopping in the Mylar versus in the graphite coating. Fitting all of the 2002 data to two different populations of muons, with different polarization rates, described the 2002 data much better than a single exponential depolarization rate. This model attributes the measured rates to muons stopping in Mylar ( $\lambda_2 = 9.3 \times 10^{-6} \text{ ns}^{-1}$ ) and muons stopping in graphite ( $\lambda_1 = 4.4 \times 10^{-4} \text{ ns}^{-1}$ ). The target has less graphite than Mylar, so the faster depolarization rate is attributed to the graphite, since the polarization at a few  $\mu\text{s}$  was 90%, not 10%. Subsequent fits to the individual 1.96 T data set and the 2.04 T data set with the two depolarization rates fixed to the values measured in the fit to all 2002 data were done. The fits resulted in the polarizations extrapolated back to zero time agreeing, because of a difference in the fraction of muons depolarizing with the two different rates. Figure 8 shows an overlay of the asymmetry analysis  $P_\mu(t)$  fit to double exponentials for the changed solenoid field data sets. The model used in the fit is:

$$P_\mu(t) = P_{\mu 1}(0)e^{-\lambda_1 t} + P_{\mu 2}(0)e^{-\lambda_2 t} \quad (9)$$

where  $P_{\mu i}(0)$  are really the product of the fraction of muons with the polarization of those muons at time zero. The fit results are summarized in Table 3.

Table 3: Results of a double exponential fit to the sum of 2002 data, and the data sets with changed solenoid field.

Description	$P_{\mu 1}(0)$	$P_{\mu 2}(0)$	$\chi^2/\text{dof}$
Sum	$-0.069 \pm 0.017$	$-0.877 \pm 0.022$	13.9/18
Set 1 (1.96 T)	$-0.081 \pm 0.007$	$-0.865 \pm 0.003$	27.7/20
Set 22 (2.04 T)	$-0.059 \pm 0.003$	$-0.888 \pm 0.003$	10.8/20

If this model is correct, the 2004 data does not have this problem since it used an Al muon stopping target. If the explanation for the different solenoid field polarization values observed

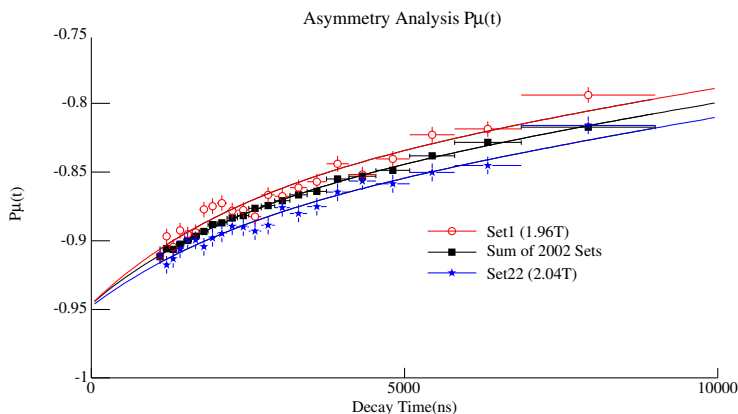


Figure 8: Overlay of the 2002 data muon polarization versus decay time from asymmetry analysis of the changed solenoid field data sets. The 1.96 T data and fit are shown as the upper red hollow circles, the 2.04 T data are shown as the lower blue stars, and the sum of all 2002 data used to determine the two decay rates are shown as the solid black squares.

in 2002 is not due to this model then there is either large unexplained difference in polarization in the data or an undiscovered bug in the analysis. Three sets of data taken in fall of 2005 were used to show that the solenoid field change was not a problem when using an Al muon stopping target. The three datasets were: 2.00 T, 1.96 T, and 2.04 T. The main result of the analysis is that there is no significant difference in the muon decay parameters, including  $P_\mu\xi$ , due to the change of solenoid field. The fit of the muon decay spectrum from the 2.04 T set to the decay spectrum from the 1.96 T set resulted in a difference in  $P_\mu\xi$  of  $0.0016 \pm 0.0015$ . The spectrum fit results are summarized in Table 4.

Table 4: Results of 2005 data solenoid field change spectrum fits for the differences in the muon decay parameters.

Data to data fit	$1000 \times \Delta\rho$	$1000 \times \Delta\delta$	$1000 \times \Delta P_\mu\xi$	$\chi^2/dof$
1.96 T A to 2.00 T	$-0.5 \pm 1.1$	$-0.0 \pm 1.8$	$1.0 \pm 2.2$	1764/1887
1.96 T B to 2.00 T	$0.1 \pm 0.8$	$-0.5 \pm 1.3$	$0.3 \pm 1.7$	1810/1887
2.04 T to 2.00 T	$0.5 \pm 0.7$	$-1.0 \pm 1.2$	$-1.3 \pm 1.5$	1903/1887
1.96 T A+B to 2.04 T	$-0.6 \pm 0.7$	$0.6 \pm 1.2$	$1.6 \pm 1.5$	1943/1887

#### 4.7.2 Dependence of depolarization on B2 setting

The fit asymmetries for four data sets at two different settings of B2, the M13 bending magnet, have been computed. The results are very encouraging for providing a definitive test of the ability of the MC to predict changes in polarization. The analysis used the 2004 version of the tracking and analysis code. Polarization weighting has been applied and the minimum  $p_t$  cut has been increased to 43 MeV/c. In summary, the fiducial is  $0.5 < \cos\theta < 0.94$ ,  $40.5 < p_{tot} < 51.5$ ,  $43. < p_t$ . The fit is an exponential with  $\lambda$  fixed at  $1.5 \times 10^{-6} \text{ ns}^{-1}$  over  $1050 < t < 9000 \text{ ns}$ . The scale factor was adjusted to give  $P_\mu(0) = -1$ . for set 49, so the polarization numbers are only relative. The results are given in Table 5. If the results are combined, the polarization difference is  $(4.27 \pm 0.51) \times 10^{-3}$ .

Table 5: Weighted asymmetry fit results.

B2 (mT)	Data set	$\mathcal{P}_\mu(0)$	$\chi^2/\text{dof}$	prob
94.6	40	$-0.999457 \pm 0.000455$	26.4/21	0.193
95.2	44	$-0.995037 \pm 0.000566$	16.2/21	0.758
94.6	49	$-1.000001 \pm 0.000495$	15.9/21	0.775
95.2	50	$-0.995876 \pm 0.000518$	14.2/21	0.859

The data results may be compared with the MC predictions obtained from characterization runs as input for the beam profiles. The results are given in Table 6. Set 44 was taken with a Be production target. Also, the TEC efficiency was quite low. The resultant prediction disagreed with the data. However, a refined analysis to compensate for the TEC efficiency change gives a consistent result.

Table 6: Predicted polarizations using characterization runs.

Data set	Runs	Target	Polarization
40	21988-90	C	0.9946
44	23707-09	Be	0.9905
49	24676-78	C	0.9964
50	24686-87	C	0.9915

### 4.7.3 TEC-in data

The intended purpose of the data taken with the TEC in was to provide an alternate validation of the MC prediction of depolarization. Using a figure-of-merit that represented the expected polarization of each muon based on the TEC measurements of position and angle, the data were divided into subsets with high and low polarization. The MC simulation predicted the difference in polarization between the two subsets would be  $\sim 12 \times 10^{-3}$ . The observed difference was only  $4 \times 10^{-3}$ . The test was hampered by very low efficiency in the TEC and thus is not considered definitive.

### 4.7.4 Enhanced PC6 stops and pure Al stops

Data were taken with the stopping distribution moved upstream in an attempt to maximize the number of stops in the PC5 and PC6 gas. The purpose was to see if it would be practical to accumulate sufficient statistics of stops in gas to make a determination of the depolarization in chamber gas. If so, a correction could be made for the small fraction of stops in gas during normal data taking. Additionally, an attempt was made to move the stopping distribution sufficiently far downstream such that the fraction stopping in the PC6 gas would be negligible. Then it might be possible to analyze these data to determine the depolarization for Al without concerns about the contamination from stops in chamber gas.

The conclusion from these studies was that it was not practical to collect sufficient statistics of stops in gas to make a determination of the depolarization in gas. However, it was realized that an even better alternative would be to make a cut in the data analysis to virtually eliminate stops in the gas. This is possible by reducing the voltage on PC5 and PC6 to 1600 V (from the usual 2050 V). Previous MC studies showed that a 2D plot of the PC5 vs PC6 pulse height is

sensitive to the energy of the muon, and thus to where the muon would stop. Figure 9 shows that a cut can select only muons with sufficient energy to stop in the Al (or Ag) target. The distribution of the left panel is similar to that observed with data.

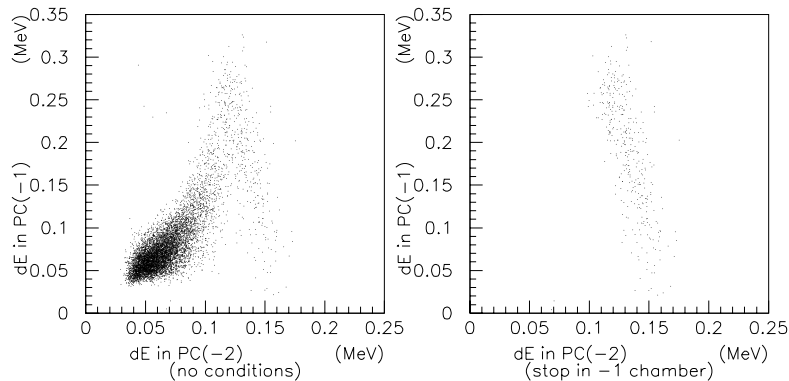


Figure 9: PC6 muon pulse width vs PC5 width, from simulation. The left panel is for muons that reach or pass through PC6. Data shows a similar distribution. The right panel is for only those muons that stop in PC6 gas.

## 5 Work In Progress

### 5.1 Improvements in analysis software

#### 5.1.1 Tracking

Considerable progress has been made in improvements to the *TWIST* tracking software. Tracking is important in *TWIST* to improve both resolution and reconstruction efficiency, and to reduce biases, by which we mean a systematic difference between the true track momentum and reconstructed momentum. A key input to the tracking is the space-time relations (STRs) which relate the measured drift time to a position in the drift cell. In the analysis of the 2002 data there was an inconsistency in end point resolution between data and simulation which is partially explained by inaccurate STRs. Our fiducial region was restricted in momentum and decay angle to regions of excellent track reconstruction efficiency and small bias in order to reduce our sensitivity to such effects. An increased fiducial means improved sensitivity to the Michel parameters in our fits.

One significant correction was the inclusion of positron energy loss in the fitted tracks. The energy loss across half of the detector stack is  $\sim 140$  keV. The correction factor was tuned on simulation, and reproduces the energy at the start of the track to  $\sim 2$  keV. This produced a significant improvement of the  $\chi^2$  of the track fits.

Our drift cells have a small asymmetry in that the sense wires are not quite centred. Bowing of some of the cell cathode foils could produce additional asymmetries. For the 2002 data symmetric STRs calculated from Garfield were used in the analysis. We have now introduced asymmetric STRs calculated with Garfield into both simulation and analysis, improved the accuracy and robustness of our tracking code, and developed a method of extracting STRs self-consistently from our data, thus enabling validation of this key quantity.

To assess the effect of the cell asymmetry, STRs calculated for a cell with one cathode foil displaced by  $150 \mu$ , were used to generate simulated monoenergetic tracks at  $p = 20, 30, 40,$  and  $50$  MeV/c. Figure 10 shows the improvement in resolution at 30 MeV/c when these tracks are analyzed with the same STR, compared to an analysis with a symmetric approximation. The

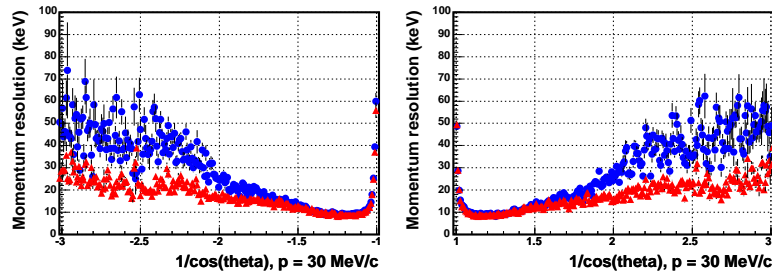


Figure 10: Momentum resolution obtained from an asymmetric STR analysis (red triangles) and from a symmetric STR analysis (blue circles) of a simulation generated using an asymmetric STR. Upstream decays are on the left panel, and downstream decays on the right.

results are different especially at large angles, which could introduce angle-dependent bias, but there are also significant improvements for small angle tracks. The calculated asymmetric STRs are currently in use in the  $\rho - \delta$  analysis of the 2004 data.

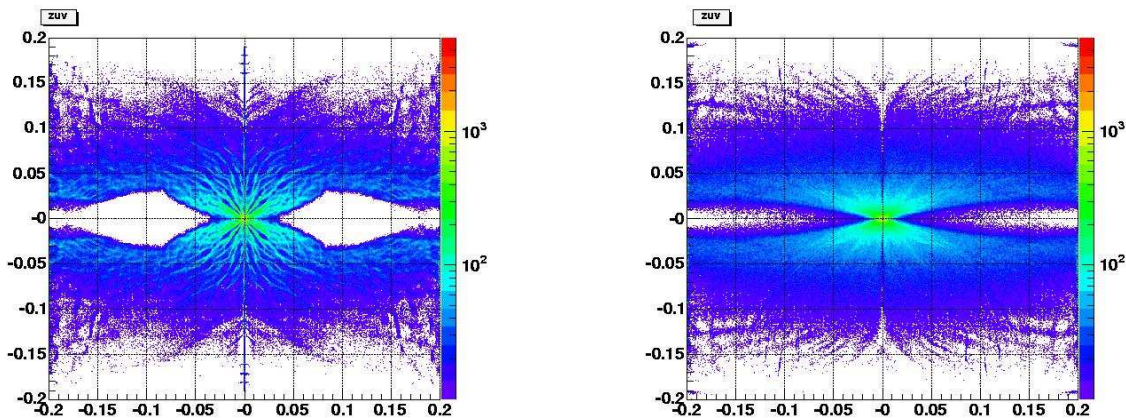


Figure 11: Hit occupancies generated from simulated data. The left panel uses the previous method of finding the point of closest time for the tracking, while the right uses an improved tracking algorithm.

The tracking code was modified using simplified and more precise cell level computations based on looking for tangents to the isochrones. Figure 11 shows the resulting improvement in the hit occupancies as a function of position in the drift cell. White areas have no occupancy; there are tracks passing through these regions, but they do not contain many points of closest approach. The filamentary artifacts apparent in the old occupancies are removed. This was required to enable the calculation of STRs from tracking residuals. In Fig. 12 one can see the substantial decrease in bias arising from this work.

The reconstruction inefficiency with the improved code can be determined from data or simulation where the muon is stopped in the upstream PCs and scintillator. Tracks are reconstructed independently in both halves of the spectrometer, and the inefficiency is the number of tracks which reconstruct in one half and fail in the other. Figure 13 shows the result of this for 2004 data together with an indication of what fiducial should be possible in the current  $\rho - \delta$  analysis. Sensitivity is increased both by raising the  $\cos(\theta)$  constraint from 0.84 to 0.96 and by increasing the the maximum momentum to 51.5 MeV/c.

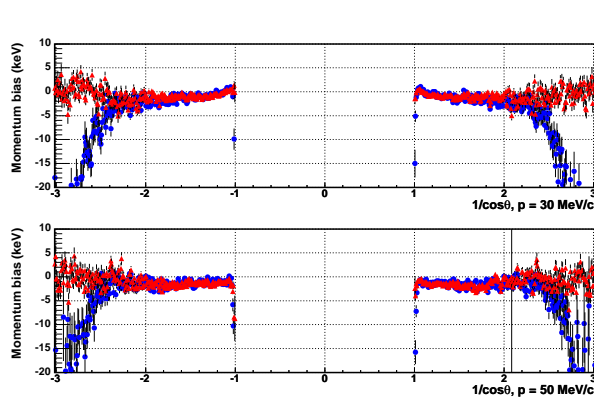


Figure 12: Track reconstruction bias for two momenta. Results from old code are in blue and from improved code in red. The improvement is seen over a wide range of momenta.

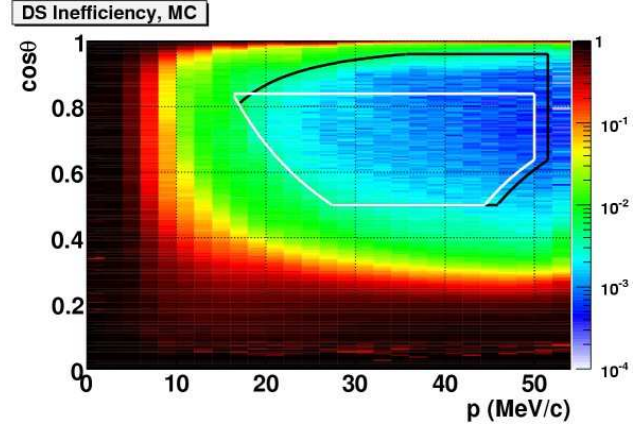


Figure 13: Track reconstruction inefficiency with improved code. The fiducial acceptances for the current analysis are drawn in black, the previous fiducial in white.

A routine to extract accurate and smooth STRs from data has just been implemented. This allows validation of the GARFIELD calculations. Uncertainties in the STRs is a possible source of discrepancy between data and simulation. In addition, there is a small error introduced when the same STRs are used in the simulation and the analysis. This bias arises because the simulation generates a drift time from the STR from the distance of closest approach, while the analysis uses the time that the first ion cluster reaches the wire. It is expected that the primary effect of this would be a worsening of the resolution, to which the Michel parameters have little sensitivity. Possible biases from this effect can be investigated by comparing the STR determined from simulation with the STR used to generate the simulation.

A further test with simulated mono-energetic tracks shows that the tracking bias with an extracted STR is almost the same as with the generating STR, (Fig. 14) but the tracking resolution is improved by  $\sim 5$  to 10 keV depending on the track's momentum (Fig. 15).

The close agreement of the data-driven STR and the Garfield STR that it was derived from demonstrates the efficacy of this procedure. Comparison of an STR derived from data with its calculated STR represents a validation of the Garfield calculation. Data-driven STRs will be used in the analysis of 2006/2007 data.

### 5.1.2 Monitoring the muon beam emittance

The leading systematic in our first measurement of  $\mathcal{P}_\mu^{\pi\xi}$  [4] came from the uncertainty in the muon polarization which is determined from the muon emittance measured by the TEC. Inconsistent values of the polarization were obtained from two different TEC measurements of the same nominal beam tune. To attack this problem, we have improved the accuracy of our beam characterization, which is done for each data set, and developed a method of monitoring changes in the beam for the data acquired after the TEC has been removed.

The electrostatic fields from the x and y modules in the TEC interfere, so the STRs are wire-dependent and complex. A pair of plates, each with a square array of 49 holes of diameter 1 mm, spaced by 10 mm, was constructed to act as a muon collimator for calibration purposes. The tracking precision of the TEC was improved through the use of data-driven STRs obtained from runs with this collimator, and through the inclusion of time walk corrections. The effect of the data-driven STRs on the muon beam emittance obtained is a shift of  $\approx 100 \mu\text{m}$  in the means of  $x$ . More recently, a larger-area collimator system using plates with 121 holes enables better TEC calibration farther from the beam axis, as much of our data for polarization systematics

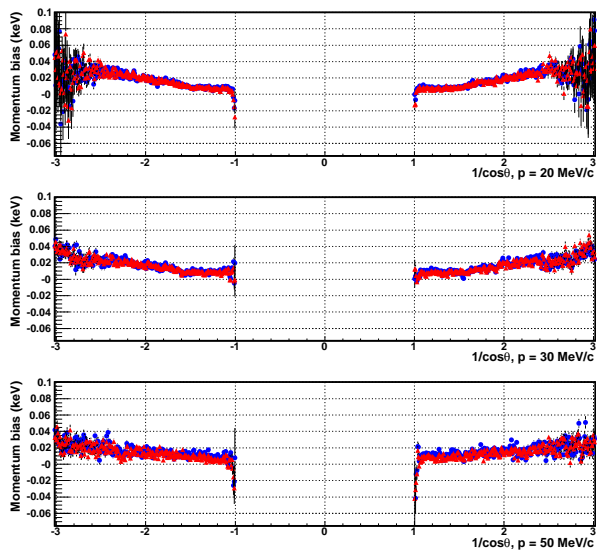


Figure 14: Comparison of tracking bias for three momenta. Red triangles are from the use of a data driven STR plus constant fixed resolution, while blue circles use a Garfield STR plus constant.

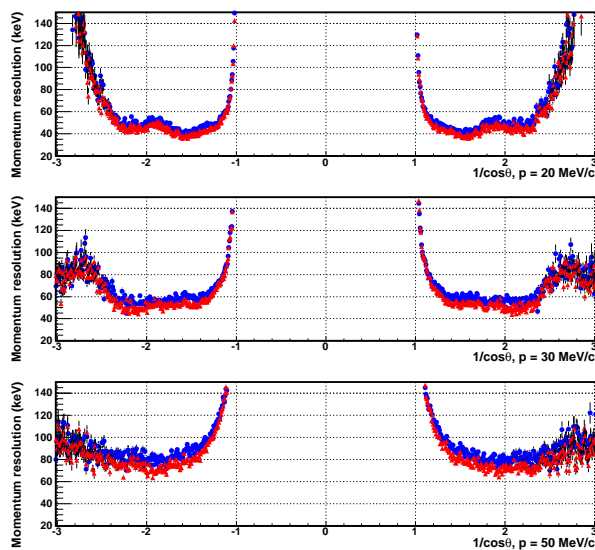


Figure 15: Comparison of tracking resolution for three momenta. Red triangles are from the use of a data driven STR plus constant fixed resolution, while blue circles use a Garfield STR plus constant.

relies on beam steered off the geometric axis.

The TEC software was expanded to allow relative alignment of the TEC with the DCs using straight (55 MeV/c) pion tracks at  $B = 0$  T. For this measurement the beam and positron scintillators were removed to reduce multiple scattering, and the events were triggered by a large downstream scintillator. A relative angular alignment of  $-2 \pm 1$  mrad in  $x$  and  $-1 \pm 1$  mrad in  $y$  was established.

Measurements of the envelope of the stopping muon beam, as it passes through the upstream half of the detector, allow us to correlate this information with the beam parameters determined by the TEC. The beam envelope is characterized by the position and width of the beam spot at each plane of the upstream half of the drift chambers after passing through the beam scintillator. Figure 16 shows the dependence of the beam spot mean  $x$  and  $y$  positions on the  $z$  position with respect to the muon stopping target, for two beams which differ in position and angle due to a change in the second M13 dipole, B2. The fit is to a damped helix, with variable initial axis, amplitude, wavelength, and damping. The variations can be validated in the simulation. The envelope fit parameters are calculated online for each data run, allowing a sensitive monitoring of possible beam and emittance changes. During setting up, the beam can be reproducibly adjusted to minimize mean transverse momentum in the solenoid, to minimize depolarization.

### 5.1.3 Chamber Time Offsets

The relative timing of all the chamber wire signals includes time offsets ( $t_0$ 's) due to electronic delays that need to be measured in a calibration procedure. This was done using dedicated alignment data taken at the beginning and end of a series of data sets. We found unexpectedly large time drifts between calibrations which resulted in a few times  $10^{-4}$  systematic in the 2002 and 2004 analyses. This  $t_0$  calibration uses 120 MeV/c pions with magnetic field off, and references all wires to a single trigger scintillator. When the solenoid is on, there is not sufficient occupancy in the outer wires to perform this calibration. If TDCs require replacement, a time-consuming magnet ramp and recalibration would be required.

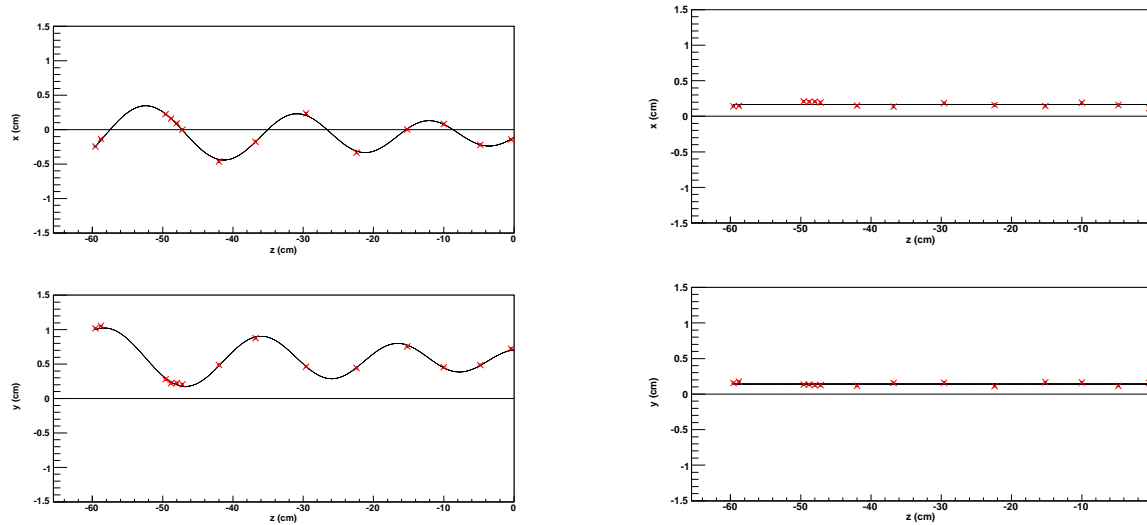


Figure 16: Mean displacement of the muon beam envelope in the upstream half of the *TWIST* spectrometer. The left panel shows  $x$  and  $y$  displacements fit to a damped helix function, for a beam steered away from the magnetic axis. The right panel is for a beam adjusted to enter along the field direction, on average, to minimize transverse momentum and thus depolarization.

To ameliorate this situation, an efficient pair of scintillators has been installed at the exit hole of the yoke for the 2006 data, complementing the annular upstream positron scintillators around the muon beam trigger scintillator. This enables us to calibrate the time offsets using normal muon decay data, and thus calibrate out any drifts, at the expense only of finding the relative timing of the two sets of scintillators with  $\sim 100$  ps accuracy. This methodology will be implemented for the 2006/2007 data analysis.

## 5.2 GEANT validation from upstream stops data

Data were taken with muons stopping at the upstream end of the detector to validate the physics for positrons in our simulation. Decay positrons from these muons traverse the entire detector. For those positrons that go through the stopping target, the detector hits in the upstream and downstream halves of the detector can be fit separately. Then the change in momentum and angle between the two measurements corresponds to the effect of the stopping target and adjacent target PCs. The distributions from data and MC can be compared and the level of agreement is used to estimate the systematic uncertainty due to possible inaccuracies in the simulation. The results are shown in Table 7.

## 5.3 Energy calibration

Energy calibration is accomplished through fitting the kinematic end point of the Michel spectrum, which is modeled in a narrow range of energy and angle by an analytic function. The angular dependence of this edge is given by  $E_{meas} = (E_{kin} - \alpha/|\cos(\theta)|)(1 + \beta)$  where  $\alpha$  is the energy loss of a track at  $0^\circ$  and  $\beta$  is a possible scale factor for uncertainties in the magnetic field and detector dimensions. The global fit is done with bins of  $0.2^\circ$ . The region  $p \geq 52$  MeV/c is selected, over which the analytic approximation is adequate. Different values  $\alpha_{up}$  and  $\alpha_{dn}$  are used for upstream and downstream decays to allow for the muon stopping position. Improved tracking at high angles has increased the angular range over which a linear  $1/\cos(\theta)$  dependence

Table 7: Differences of momentum and angle between simulation and data for positrons traversing both halves of the *TWIST* detector, from muons stopping near the upstream end.

$\Delta p \cos \theta$ : (range $[-1, 1]$ MeV/c for peak and FWHM)			
	peak (keV/c)	FWHM (keV/c)	tail rate
MC	$-29.65 \pm 0.04$	$141.64 \pm 0.04$	$0.01420 \pm 0.00004$
data	$-28.4 \pm 0.1$	$155.9 \pm 0.1$	$0.0142 \pm 0.0001$
difference	$1.3 \pm 0.1$	$14.3 \pm 0.1$	$0.0000 \pm 0.0001$
$\Delta \theta$ : (range $[-0.25, 0.25]$ rad for peak and FWHM)			
	peak (mrad)	FWHM (mrad)	tail rate
MC	$-0.581 \pm 0.007$	$29.159 \pm 0.007$	$0.00513 \pm 0.00003$
data	$-0.97 \pm 0.02$	$29.75 \pm 0.02$	$0.00497 \pm 0.00007$
difference	$0.39 \pm 0.02$	$0.59 \pm 0.02$	$0.00016 \pm 0.00008$ (3%)

is observed. The sum  $\alpha_{sum} = \alpha_{up} + \alpha_{dn}$  is not constrained, and must be consistent with the energy loss  $\Delta E$  of positrons passing through the full target and target PC's obtained from upstream stops data.

Figure 17 shows the quality of the fits, and the resulting angular dependence.

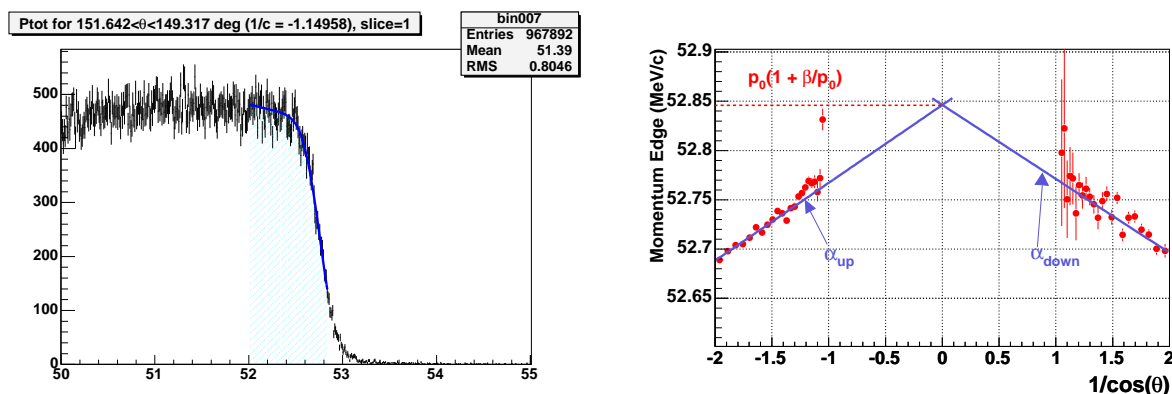


Figure 17: Left panel: Fit to the endpoint. Right panel: Angular dependence of the endpoints. Red points are from fits to individual angular ranges, while lines for  $\alpha_{up}$  and  $\alpha_{dn}$  are obtained from a constrained global fit.

The accuracy with which our magnetic field is measured implies an uncertainty of  $\sim 2.5$  keV in  $\beta$ ; additional uncertainty can arise from the approximations inherent in the energy calibration model. In fact we find  $\beta \sim 20$  keV, and there is disagreement of the same order between  $\alpha_{sum}$  and  $\Delta E$ . Non-zero  $\beta$ s are in fact predicted by our simulation. These problems are of order 10% of the resolution and the energy loss through the target, so there is some sensitivity to modeling details. Improving this to the required level remains a challenge, which will likely require increased sophistication in the energy calibration model.

## 5.4 Analysis for $\rho$ and $\delta$ from 2004 data

*TWIST* is currently reanalyzing the data taken in the fall of 2004 for our next measurements of  $\rho$  and  $\delta$ . This is the same data as was used for the recent measurement of  $\mathcal{P}_\mu^\pi \xi$ , seven sets of data containing about 1.6 billion muon decays. New MC sets have been produced to match each data set with about three times as many events. As already mentioned, there have been a number

of improvements to the simulation and analysis since the previous round, including accounting for the asymmetric cell geometry, improved cell hit calculations, and compensating for positron energy loss in the helix fits. The fiducial region has been significantly enlarged as well, increasing the number of events available and improving our sensitivity to the Michel parameters, both of which decrease the statistical uncertainties of the measurement. The new fiducial region should result in statistical uncertainties of about  $2 \times 10^{-4}$  for  $\rho$  and about  $3 \times 10^{-4}$  for  $\delta$ .

The systematic uncertainties are also being re-evaluated. Many have been significantly reduced compared to previous measurements. Experience has allowed us to improve our techniques for measuring the systematics, and that combined with the increased MC statistics and the enlarged fiducial region allow us to improve them. Some improvements are already complete, while others are ongoing. They will be discussed in a subsequent section along with projected systematics for future analyses.

## 6 Toward final results for TWIST

### 6.1 2006 data

The 2006 data run is well along as this application is being submitted. Several significant improvements have been implemented; these are essential to achieve the ultimate goals for *TWIST*. The quadrupole steering (discussed in Section 3.3) has enabled control of the position and angle of the muon beam. The modular construction of the *TWIST* detector (discussed in Section 3.1) allowed a revised geometry to break an annoying degeneracy that degraded the momentum resolution for certain momenta and limited the allowed fiducial region. The design of the detector also permitted an efficient switch from an aluminum stopping target to a silver target.

The operating conditions for PC5 and PC6 were modified, such that muons that stop in the PC6 gas can be rejected. Thus one source of systematic for the  $\mathcal{P}_\mu^\pi \xi$  measurement will be reduced to a negligible level.

A new diagnostic (see Section 5.1.2) was devised that characterizes the muon beam envelope in the detector. This has become a powerful tool for measuring and reducing the transverse momentum of the beam. It also permits a validation that the simulation properly reproduces different conditions for the data.

The quantity of data for a single condition (a data set) has been increased by a factor of three to  $\sim 10^9$  events per set (or super-set). The sets already taken with an Al stopping target are shown in Table 8.

Table 8: List of data sets, conditions, and runs taken prior to September 2006 with an Al muon stopping target. Runs of 2 GB typically contain of order  $10^6$  events.

	runs
Set 60, high rate	1222
Set 61, nominal 1	900
Set 62, 3/4 stop	915
Set 63, mis-steered beam 1	888
Set 64, TEC in data set	1852
Set 65, upstream stops 2.0 T	456
Set 66, nominal 2	890
Set 67, mis-steered beam 2	913

Table 9: Projected statistical uncertainties for 3 super-sets from 2006 and from our final statistics, compared to previous data with smaller sets. Units are  $10^{-3}$ .

	2004 stat/set	2006, 3 super-sets	Final
$\rho$	0.36	0.13	0.10
$\delta$	0.64	0.23	0.22
$\mathcal{P}_\mu^\pi \xi$	0.77	0.28	0.30

Taking only sets 61, 62, and 66, the statistical precision on the Michel parameters can be estimated from the preliminary results for the reanalysis of the 2004 data (Section 5.4). In Table

9, the first column of numbers is the statistical uncertainty per (smaller) set using increased MC statistics and an expanded fiducial compared to the published results. The next columns are the projected uncertainty for three super-sets of AI data and the final goals from the 2004 NSERC application.

The numbers show that the statistical goals have been met. However, there is some question about the quality of the data. It was discovered that two stainless steel wrenches were left on the lower cover plate inside the detector during the AI data. The amount of distortion of the magnetic field due to these wrenches is being evaluated.

## 6.2 Projected systematics

The 2004 NSERC application included a table of systematic error estimates from the analysis of the 2002 data and goals for the 2004-5 runs and the final data. Subsequently, the analysis of the 2004 data for  $\mathcal{P}_\mu^\pi \xi$  showed that the polarization related systematics were not under control at the hoped-for level. Much was learned from the 2004 data and several improvements were tested during 2005 (Section 4.7). The reanalysis of the 2004 data to extract  $\rho$  and  $\delta$  is in progress, so few new results are available at this time. Thus the following discussion is mostly qualitative.

The values for the past, present, and future are summarized in Table 10. The first three columns of numbers are given for reference from our publications. For the 2002 data, the leading relevant systematic uncertainties for  $\rho$  and  $\delta$  were the categories of chamber response and positron interactions. The systematic uncertainty for  $\mathcal{P}_\mu^\pi \xi$  from the 2004 data was dominated by uncertainties in two of the polarization terms. The projections for the reanalysis of the 2004 data for  $\rho$  and  $\delta$  are mostly based on sensitivities from the 2002 analysis, so they are not really independent information.

The chamber response systematic is not expected to be important for the 2006 data. From the discussion in Section 4.6, there are several elements that contribute: dead zone, foil bulge, upstream-downstream efficiency differences, cell asymmetry,  $t_0$  variations, and STRs (density). For the 2004  $\mathcal{P}_\mu^\pi \xi$  result, the uncertainty in chamber response was dominated by the contribution from  $t_0$ . An improved technique and more frequent  $t_0$  calibrations have reduced this contribution (Section 5.1.3). The other contributions were already small or have also been reduced by improved running conditions or analysis procedures.

The systematic uncertainty for positron interactions, which was a leading uncertainty for the published results for  $\rho$  and  $\delta$ , should not be a problem for the 2006 data. This projection is based partly on the results presented in Section 5.2 where there is no discrepancy between data and MC for hard interactions. If the energy calibration compensates for any difference between data and MC for the peak energy loss, then the systematic uncertainty for interactions should not be significant. Some contributions remain. There is a difference in the width of the energy loss distributions, which is presumably a difference in resolution between data and MC. There is also a non-zero difference in both the peak and tail for scattering. The projected uncertainty is based on previous estimates for these contributions.

The decay parameter systematic uncertainty category for energy calibration is dominated by the uncertainty in energy calibration itself. This is an area of active study, and while we have made recent progress, the projection for systematic uncertainty is speculative. The minimum systematic uncertainty is that due to the statistical limitation of the determination of the energy calibration parameters for a given data or MC set. This was the only source of uncertainty included for previous analyses. This contribution will be reduced by at least a factor of  $\sqrt{3}$  due to the increase in statistics per set.

There is a difference in the energy calibration parameters for data and MC, but the underlying reasons are yet to be determined. The energy calibration procedure tends to suppress the difference, but any residual would be a non-statistical contribution to the energy calibration systematic uncertainty. Also if the assumptions about the angle-dependent parameters of the energy calibration are not accurate, systematic errors could result. Quantitative assessments of these effects are difficult and have not been made, but there are indications that they could be

Table 10: Table of systematic uncertainties, showing progress toward our goals. Blank entries indicate no applicable systematic, while “neg” means the value is negligible. The units are  $10^{-3}$ .

	2002 $\rho$	2002 $\delta$	2004 $\mathcal{P}_\mu^\pi\xi$	2004 $\rho$	2004 $\delta$	2006 $\rho$	2006 $\delta$	2006 $\mathcal{P}_\mu^\pi\xi$
	published			preliminary		predicted		
Chamber response	0.51	0.56	1.0	0.02	0.13	neg	0.1	0.1
Stopping tgt. thickness	0.49	0.37						
Positron interactions	0.46	0.55	0.3	0.38	0.24	0.1	0.1	0.1
Alignment	0.22	0.61	0.3	0.04	0.01	neg	neg	neg
Energy calibration	0.20	0.29	0.2	0.11	0.22	0.09	0.13	0.16
Theory rad. correction	0.20	0.10	0.1	0.20	0.10	0.2	0.1	0.1
Track selection alghm	0.11							
Muon beam stability	0.04		0.2	0.05	0.09	neg	neg	neg
Up/down efficiency		0.04	0.2				neg	neg
Fringe field depol.			3.4					0.5
Stopping material depol.			1.2					0.5
Prod. tgt. depol.			0.2					neg
Background muons			0.2					neg
$\eta$			0.1					0.1
Total	0.97	1.12	3.8	0.46	0.43	0.24-?	0.22-?	0.75-?
$\eta(\rho)$	0.23			0.23		0.23		
Goals from previous NSERC						0.26	0.32	0.30

come the leading contributions to the systematic uncertainty for  $\rho$  and  $\delta$  without improvements to the energy calibration procedures. However, we are optimistic that the systematic uncertainty can be reduced to the statistical contribution and those values are entered in Table 10 for the final results.

Because the energy calibration only matches data and MC at the endpoint, all lower momenta must be corrected using an assumed energy dependence. From the upstream stops data, the match between data and MC at lower momenta has been determined and the systematic uncertainty due to any uncorrected mismatch is negligible.

For the  $\mathcal{P}_\mu^\pi\xi$  result from the 2004 data, the estimate of systematic uncertainty due to a difference between the chamber efficiency in the upstream and downstream halves of the detector was based on an indirect measure of efficiency. Recent direct measures of the efficiency show that the efficiencies match at the level of  $10^{-3}$ , so that this systematic uncertainty will be negligible.

The systematic uncertainty in depolarization due to the fringe field can be estimated from the agreement between relative polarizations from data and MC for sets 40, 44, 49, and 50 (Table 6). The precision of the comparison is limited by the statistical precision of the polarization from the data analysis to be at the level of  $0.5 \times 10^{-3}$ .

The  $\mu$ SR experiment should resolve any uncertainty about the form of the depolarization in Al and Ag. Presumably it is exponential. The experiment should also mostly eliminate the possibility of a faster depolarization component. Application of the PC5/PC6 energy loss cut (Section 4.7.4) will eliminate muons that stop in the PC6 gas. Then the uncertainty in  $\mathcal{P}_\mu^\pi\xi$  due to depolarization in the stopping target will be only the statistical uncertainty in the extrapolation. For the 2004 data, this was  $1 \times 10^{-3}$ . From the 2006 data the error should be reduced by at least a factor of 2.

The projected total systematic uncertainties for  $\rho$  ( $0.24 \times 10^{-3}$ ),  $\delta$  ( $0.22 \times 10^{-3}$ ), and  $\mathcal{P}_\mu^\pi\xi$  ( $0.75 \times 10^{-3}$ ) meet the design goals of *TWIST* for a factor of ten improvement in each parameter. With the unprecedented increase in statistics for the determination of these parameters, the

sensitivity to systematic errors will also be unprecedented. The “?” symbols in the projected totals account for the possibility that a surprise source of systematic error will be revealed.

### 6.3 Known challenges

The analysis software for *TWIST* continually evolves as new challenges are discovered and addressed. Recent developments have been summarized in Section 5.1. We have always known that *TWIST* will be a systematics dominated experiment. To meet the goals for systematics uncertainties presented in the preceding section, much work lies before us; this research proposal describes the most important tasks. Known areas of development include the formalism for energy calibration. Implementing STRs derived directly from data should improve the match between data and MC. Another area for study is the match between data and MC for quantities that measure the quality of the MC to simulate the interactions of positrons with materials in the detector. An effort to develop a GEANT4 based simulation of the experiment has recently progressed to the point that direct comparisons with our GEANT3 simulation are possible. A decision on which code to use for the final MC will be based on a comparison of the level of agreement with data and the ability to tweak the code as needed.

We are quite optimistic that major progress has been made in reducing the polarization-related systematic uncertainties, which are essential for an improved result for  $\mathcal{P}_\mu^\pi \xi$ . We believe we are now in a position to validate the MC predictions for depolarization in the solenoidal fringe field. We also believe we can demonstrate an understanding of the depolarization in the stopping target. However, it will take time to fully evaluate the improvements and to convince ourselves that these uncertainties are under control.

## 7 Summary

The challenges of a high precision determination of muon decay parameters are not to be underestimated. When *TWIST* was proposed, it was not clear that those challenges could be overcome. While it is still not completely certain that there will be no surprises in our evaluations of systematic uncertainties, many problems have been solved and the methods to accomplish our ultimate goals are in place and, so far, working well. We have learned a great deal from the first rounds of analysis about where the main weaknesses lie. We know how to use our high precision detector to the limits of its capabilities. We have found and corrected weaknesses in control of depolarization. While the plan for analysis of data via comparison to simulation posed certain risks, we have been able to devise ways to verify the simulation to the required precision. In summary, we see no reason that *TWIST* should not be able to achieve its original goal of one order of magnitude increase in precision for the muon decay (Michel) parameters  $\rho$ ,  $\delta$ , and  $\mathcal{P}_\mu \xi$ . An improved intermediate result for  $\rho$  and  $\delta$  should be published within six months. With our capable team of graduate students, postdoctoral fellows, and other researchers, we are now collecting the last sets of data for the experiment. The end-of-data-taking milestone should be in 2007. We will then proceed with final analyses in 2007-08, and complete them by 2010. A stable and adequate level of funding as outlined in this application is necessary for us to continue to produce these excellent results.

## References

- [1] L. Michel, Proc. Phys. Soc. **A63**, 514 (1950).
- [2] TWIST Collaboration, J. R. Musser *et al.*, Phys. Rev. Lett. **94**, 101805 (2005).
- [3] TWIST Collaboration, A. Gaponenko *et al.*, Phys. Rev. D **71**, 071101(R) (2005).
- [4] TWIST Collaboration, B. Jamieson *et al.*, Phys. Rev. D **74**, 072007 (2006).
- [5] W. Fetscher, H.-J. Gerber, and K. F. Johnson, Phys. Lett. **B173**, 102 (1986).
- [6] W.-M. Yao *et al.*, Journal of Physics **33**, 1 (2006).
- [7] C. Bouchiat and L. Michel, Phys. Rev. **106**, 170 (1957).
- [8] A. Sirlin, Phys. Rev. **108**, 844 (1957).
- [9] A. B. Arbuzov, Phys. Lett. **B524**, 99 (2002).
- [10] A. Arbuzov, A. Czarnecki, and A. Gaponenko, Phys. Rev. **D65**, 113006 (2002).
- [11] A. Arbuzov and K. Melnikov, Phys. Rev. **D66**, 093003 (2002).
- [12] C. Gagliardi *et al.*, Phys. Rev. D (2005).
- [13] R. J. Erwin *et al.*, arXiv:hep-ph/0608163, 2006.
- [14] S. Profumo *et al.*, arXiv:hep-ph/0608064, 2006.
- [15] A. Pifer, T. Bowen, and K. Kendall, Nucl. Instr. and Meth. **135**, 39 (1976).
- [16] R. L. Henderson *et al.*, Nucl. Instr. and Meth. A **548**, 306 (2005).
- [17] J. Hu *et al.*, Nucl. Instr. and Meth. A **566**, 563 (2006).
- [18] A. Jodidio *et al.*, Phys. Rev. **D34**, 1967 (1986).
- [19] A. Jodidio *et al.*, Phys. Rev. **D37**, 237(E) (1988).
- [20] M. Senba, J. Phys. B: At. Mol. Opt. Phys. **31**, 5233 (1998).
- [21] D. G. Fleming and M. Senba, Atomic Physics with Positrons, ed. J.W. Humberston and E.A.G. Armour, Plenum, 1987.
- [22] F. James, Nucl. Instr. and Meth. **211**, 45 (1983).
- [23] G. Lutz, Nucl. Instr. and Meth. **A273**, 349 (1988).
- [24] J. Korringa, Physica **16**, 601 (1950).
- [25] S. Cox *et al.*, Physica B **289-290**, 594 (2000).
- [26] R. Kubo and K. Tomita, J. Phys. Soc. Jpn. **9**, 888 (1954).
- [27] I. Beltrami *et al.*, Phys. Lett. **B194**, 326 (1987).